Journal of Sound and Vibration (2001) **239**(2), 297–320
doi:10.1006/jsvi.2000.3169, available online at http://www.idealibrary.com on IDEAL®

DYNAMIC STIFFNESS FORMULATION, FREE VIBRATION AND WAVE MOTION OF HELICAL SPRINGS

J. LEE†

Graduate School of Automotive Engineering, Kookmin University, 861-1, *Chongnung-dong, Songbuk-gu, Seoul*, 136-702, *Korea*

AND

D. J. THOMPSON

*Institute of Sound and Vibration Research, University of Southampton, Highfield, Southampton SO*17 1*BJ, England. E-mail: djt@isvr.soton.ac.uk*

(*Received* 25 *November* 1999, *and in final form* 2 *June* 2000)

A coil spring can only be treated as a simple massless force element at low frequencies, the effects of internal resonances leading to significant dynamic stiffening. For an automotive suspension spring this occurs at frequencies as low as about 40 Hz. This paper presents an efficient method for calculating the dynamic stiffness of a helical coil spring. The partial differential equations of motion are used to derive the relation between wavenumber and frequency along with the associated wave shapes. By expressing the response in terms of these waves, the dynamic stiffness matrix is assembled. Natural frequencies are obtained from the reduced stiffness matrix, allowing for different boundary conditions, making use of the Wittrick–Williams algorithm. The results of the dynamic stiffness method are compared with those of the transfer matrix method and the finite element method. The nature of the wave propagation is also investigated. Although at low frequencies four wave types propagate, above a particular frequency only two propagating waves remain. These are composite waves which are excited by both axial and transverse motion. For lower values of helix angle an intermediate frequency range exists where six propagating waves can occur.

1. INTRODUCTION

The helical spring is a very common and important element in many machines and vehicles. In dynamic analyses, such springs as well as dampers are often treated as simple massless force elements. However, as the frequency range of interest increases, such an approach is not suitable for the prediction of the dynamic behaviour of the system. In particular, above a certain frequency, internal resonances of the spring have to be taken into account. For a coil spring with dimensions that are typical for application in an automotive suspension, for example, the dynamic stiffness is found to increase sharply at frequencies as low as about 40 Hz due to such internal resonances. This paper gives an efficient method for calculating the dynamic stiffness of a helical spring.

Already a 100 years ago, Love [1] gave the equations of motion for a coil spring. However, these 12th order differential equations could not be solved analytically. In the 1930s, Timoshenko [2] derived the rigidity of the compression, lateral and shear deflections

†Work carried out while a visiting research fellow at ISVR, Southampton.

0022-460X/01/020297 + 24 $35.00/0

for a coil spring in order to explain the bounds of stability of a compressed helical spring due to lateral buckling.

Wittrick's [3] paper of 1966 is a classic treatise on the behaviour of helical springs. Prior to this, as given by Wahl [4], in analyses of the propagation of extensional waves along the axis of a helical spring, it was assumed that the coupling between extension of the spring and rotation about its axis could be ignored. Wittrick treated the helical spring as a Timoshenko beam including shear deformation and rotational inertia and obtained a set of 12 linear coupled partial differential equations. These were the most complete equations at the time, and apart from minor corrections, have been used by a number of authors since. He obtained approximate solutions in several ways but did not obtain an exact solution.

Jiang *et al.* [5, 6] obtained non-linear equations of motion and from them linearized equations for the vibration of a spring. They studied the coupling between axial and torsional motion in more detail than Wittrick, deriving the complex form of the oscillations of the spring in the time domain due to the interaction and superposition of the component waves.

Sinha and Costello [7] used a finite difference technique and the method of non-linear characteristics to solve numerically the non-linear partial differential equations in the time domain. This study too is limited to axial and torsional motion of the spring.

Banerjee and Williams [8] gave an exact dynamic stiffness matrix for the coupled extension and torsion of a member of which a helical spring is a good example. In reference [9] it is shown that the natural frequencies of such a system for different boundary conditions are related. In particular, the non-zero extensional/torsional natural frequencies for the free–free case are identical to those for the clamped–clamped case. It will be seen in this paper that if coupling with lateral motion is significant, this equality is only approximate.

It is not a simple matter to extend the above analyses to include out-of-plane motion of the spring. The axial and torsional motions can be likened to those of a simple rod, but coupling between the different equations of motion makes such an analogy less useful for the out-of-plane motion. However, with the aid of digital computers it is possible to solve the differential equations as given by Love or Wittrick.

Mottershead [10] developed special finite elements for solving the differential equations. He obtained element displacement functions by integrating the differential equations. The elements so obtained may be one or more turns of the spring in length or a fraction of a turn. For static problems his elements provide exact solutions whilst for dynamics the natural frequencies are unaffected by mesh density provided that sufficient master degrees of freedom are specified. Mottershead also performed experiments on two small clamped–clamped springs, the results of which have been used by other researchers to test their theories. As well as predominantly extensional and torsional modes, "snaking" modes that also involve transverse motion were found that can explain the side wear of coils under axial loading. Such modes cannot be detected by using simple theories.

Another approach is the transfer matrix method, employed by Pearson [11]. He extended the partial differential equations of motion for a helical spring to include the effects of a static axial preload. The transfer matrix was obtained from the differential equations by a series expansion. This series does not converge if the spring is too long, so usually the spring is sub-divided into 2^m equal segments. The natural frequencies were found as the zeroes of the determinant of a 6×6 frequency-dependent matrix. An iterative method was used for this. Pearson shows the dependence of the natural frequencies on axial load, helix angle, number of turns, etc.

Yildirim [12] also used the transfer matrix approach, making use of the Cayley–Hamilton theorem to develop an algorithm which allows the transfer matrix to be

determined with improved precision. This is especially important for long springs. In reference [13] Yildirim concentrated on determining the natural frequencies for arbitrarily shaped springs. In reference [14] an efficient method for determining the natural frequencies is developed.

In reference [15], Pearson and Wittrick used the dynamic stiffness method to find an exact solution for the natural frequencies of a coil spring based on Bernoulli–Euler beam theory and an adaptation of the Wittrick–Williams algorithm [16]. Although efficient and analytically exact, this work does not include shear deformation in the wire, important at high frequencies.

In this paper the governing partial differential equations of motion of a helical spring are first obtained, based on Timoshenko beam theory and Frenet's formulation for curved systems, as in references [10–12]. The theory is applied to helical springs wound using wire with a circular cross-section. From these equations the dispersion relation, linking wavenumber and frequency for each wave, is derived and the nature of the various waves is studied. The variation in the dispersion relation with helix angle is investigated. By a summation of waves, a frequency-dependent dynamic stiffness matrix, **K**, is determined that links the six degrees of freedom at each end of the spring to the six forces/moments at each end. After applying suitable constraints, the frequencies at which the determinant of **K** vanishes give the natural frequencies of the spring. In fact, the Wittrick–Williams method [16] is used to determine the natural frequencies more efficiently. Moreover, the dynamic stiffness matrix can be used directly as an "exact" element in a model of a more complicated structure, for example a vehicle. The method allows an efficient calculation to be made which accounts for the complex modal behaviour of springs at high frequency. The method is applied to a typical spring from a car suspension in section 3.

2. THEORETICAL BACKGROUND AND FORMULATION

2.1. EQUATIONS OF THE HELIX

For clarity, the equations of a helix are introduced first and used to derive the equations of motion of a helical spring. Figure 1 shows a helical coil spring, the axis of which lies along the x-axis. The helix radius is R and the helix angle is α. The variable s is used to measure the distance along the wire and is related to the angle ϕ by

$$\phi = s\cos\alpha/R. \tag{1}$$

The global (x, y, z) co-ordinates are related to ϕ by

$$x = R\phi\tan\alpha, \quad y = R\cos\phi, \quad z = R\sin\phi. \tag{2}$$

At any point on the helix, local co-ordinates are defined as shown in Figure 2, with $\hat{\mathbf{u}}$ radial, $\hat{\mathbf{w}}$ tangential and $\hat{\mathbf{v}}$ binormal to the other directions. The displacements (u, v, w) in these local co-ordinates are related to those in global co-ordinates (u_x, u_y, u_z) by

$$\begin{Bmatrix} u \\ v \\ w \end{Bmatrix} = \begin{bmatrix} 0 & -\cos\phi & -\sin\phi \\ \cos\alpha & \sin\alpha\sin\phi & -\sin\alpha\cos\phi \\ \sin\alpha & -\cos\alpha\sin\phi & \cos\alpha\cos\phi \end{bmatrix} \begin{Bmatrix} u_x \\ u_y \\ u_z \end{Bmatrix} = [\mathbf{Q}] \begin{Bmatrix} u_x \\ u_y \\ u_z \end{Bmatrix}. \tag{3}$$

Similar equations apply for rotations, forces and moments.

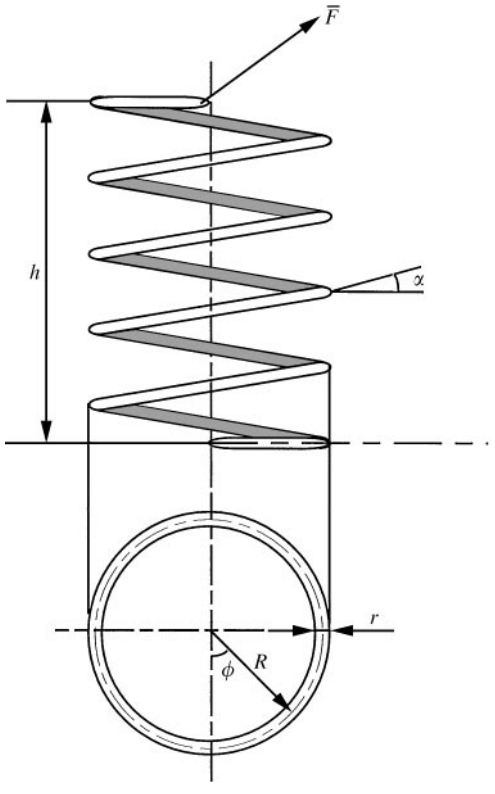

Figure 1. Schematic view of a helical spring.

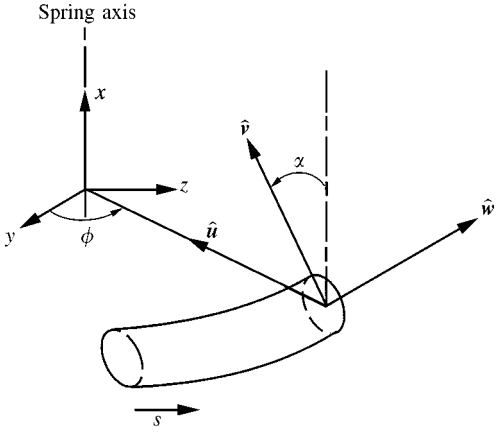

Figure 2. Co-ordinate system of a helical spring.

Frenet formulation [17] allows all the displacements and resultant forces to be given as functions of s. The curvature κ and tortuosity τ of the helix are defined by

$$\kappa = \frac{\cos^2 \alpha}{R}, \quad \tau = \frac{\sin \alpha \cos \alpha}{R}. \tag{4}$$

The relations between these parameters and the three unit vectors [14] can be written in matrix form as

$$\frac{\partial}{\partial s}\begin{Bmatrix}\hat{\mathbf{u}}\\ \hat{\mathbf{v}}\\ \hat{\mathbf{w}}\end{Bmatrix}=\begin{bmatrix}0 & \tau & -\kappa\\ -\tau & 0 & 0\\ \kappa & 0 & 0\end{bmatrix}\begin{Bmatrix}\hat{\mathbf{u}}\\ \hat{\mathbf{v}}\\ \hat{\mathbf{w}}\end{Bmatrix}. \tag{5}$$

2.2. EQUILIBRIUM EQUATIONS

Consider the situation in which the spring is subjected to an arbitrary dynamic load $\bar{\mathbf{F}}$, as shown in Figure 1. Then at any cross-section the wire is subjected to three components of force P_u, P_v, P_w and three moments M_u, M_v, M_w about the $\hat{\mathbf{u}}, \hat{\mathbf{v}}$ and $\hat{\mathbf{w}}$ directions (see Figure 2). These forces and moments result in the linear and rotational displacements of the wire and cause the coupling effects of motion of the spring. It will be assumed that the cross-section of the wire has two axes of symmetry which coincide with the directions $\hat{\mathbf{u}}$ and $\hat{\mathbf{v}}$. Suppose that the components of the linear displacements $\boldsymbol{\delta}$, rotations $\boldsymbol{\theta}$, concentrated forces $\mathbf{P}$ and moments $\mathbf{M}$ at position s are defined by

$$\begin{Bmatrix}\boldsymbol{\delta}\\ \boldsymbol{\theta}\\ \mathbf{P}\\ \mathbf{M}\end{Bmatrix}=\begin{bmatrix}\delta_u & \delta_v & \delta_w\\ \theta_u & \theta_v & \theta_w\\ P_u & P_v & P_w\\ M_u & M_v & M_w\end{bmatrix}\begin{Bmatrix}\hat{\mathbf{u}}\\ \hat{\mathbf{v}}\\ \hat{\mathbf{w}}\end{Bmatrix}. \tag{6}$$

Differentiating equation (6) by the length measured along the helix s yields

$$\frac{\mathrm{d}}{\mathrm{d}s}\begin{Bmatrix}\boldsymbol{\delta}\\ \boldsymbol{\theta}\\ \mathbf{P}\\ \mathbf{M}\end{Bmatrix}=\left(\frac{\partial}{\partial s}\begin{bmatrix}\delta_u & \delta_v & \delta_w\\ \theta_u & \theta_v & \theta_w\\ P_u & P_v & P_w\\ M_u & M_v & M_w\end{bmatrix}\right)\begin{Bmatrix}\hat{\mathbf{u}}\\ \hat{\mathbf{v}}\\ \hat{\mathbf{w}}\end{Bmatrix}+\begin{bmatrix}\delta_u & \delta_v & \delta_w\\ \theta_u & \theta_v & \theta_w\\ P_u & P_v & P_w\\ M_u & M_v & M_w\end{bmatrix}\left(\frac{\partial}{\partial s}\begin{Bmatrix}\hat{\mathbf{u}}\\ \hat{\mathbf{v}}\\ \hat{\mathbf{w}}\end{Bmatrix}\right). \tag{7}$$

Timoshenko beam theory [2] gives the relationship between displacements and forces as

$$\frac{\mathrm{d}}{\mathrm{d}s}\begin{Bmatrix}\boldsymbol{\delta}\\ \boldsymbol{\theta}\\ \mathbf{P}\\ \mathbf{M}\end{Bmatrix}=\begin{bmatrix}\dfrac{P_u}{GA\gamma}+\theta_v & \dfrac{P_v}{GA\gamma}-\theta_u & \dfrac{P_w}{EA}\\ \dfrac{M_u}{EI_u} & \dfrac{M_v}{EI_v} & \dfrac{M_w}{GJ}\\ 0 & 0 & 0\\ P_v & -P_u & 0\end{bmatrix}\begin{Bmatrix}\hat{\mathbf{u}}\\ \hat{\mathbf{v}}\\ \hat{\mathbf{w}}\end{Bmatrix}, \tag{8}$$

where E is the Young's modulus, G the shear modulus, A the cross-sectional area of the wire, γ is the shear area correction, I_u and I_v are the second moments of area of the section about the directions $\hat{\mathbf{u}}$ and $\hat{\mathbf{v}}$ and J is the St. Venant torsion constant. In this paper, the theory is applied to a spring composed of a circular wire. In this case $I_u = I_v$ and $J = I_w$ the polar moment of area about the direction $\hat{\mathbf{w}}$. More advanced beam theories include the effects of initial twist and curvature (see, e.g., reference [18]). For circular sections, the effect of initial twist is eliminated. The remaining initial curvature effects introduce extension-bending, extension-shear, bending-shear and twist-shear coupling terms, that are proportional to κ, as well as introduce quadratic correction terms to the stiffness. However, these effects are neglected here for simplicity, as in previous work [3, 10–12], since not all such coupling terms are available in analytical form.

By substituting equations (5) and (8) into equation (7) and rearranging, the governing partial differential equations for the static equilibrium are obtained as follows:

$$\frac{\partial}{\partial s}\begin{Bmatrix}\boldsymbol{\delta}\\ \boldsymbol{\theta}\\ \mathbf{P}\\ \mathbf{M}\end{Bmatrix} = \begin{bmatrix} \dfrac{P_u}{GA\gamma} + \theta_v + \tau\delta_v - \kappa\delta_w & \dfrac{P_v}{GA\gamma} - \theta_u - \tau\delta_u & \dfrac{P_w}{EA} + \kappa\delta_u \\ \dfrac{M_u}{EI_u} + \tau\theta_v - \kappa\theta_w & \dfrac{M_v}{EI_v} - \tau\theta_u & \dfrac{M_w}{GI_w} + \kappa\theta_u \\ \tau P_v - \kappa P_w & -\tau P_u & \kappa P_u \\ P_v + \tau M_v - \kappa M_w & -P_u - \tau M_u & \kappa M_u \end{bmatrix} \begin{Bmatrix}\hat{\mathbf{u}}\\ \hat{\mathbf{v}}\\ \hat{\mathbf{w}}\end{Bmatrix}, \tag{9}$$

Upon rearranging by components of displacements and forces, this can be written as

$$\frac{\partial}{\partial s}\begin{Bmatrix}\boldsymbol{\delta}\\ \boldsymbol{\theta}\\ \mathbf{P}\\ \mathbf{M}\end{Bmatrix} = \begin{bmatrix}\mathbf{S}_{11} & \mathbf{S}_{12}\\ \mathbf{0} & \mathbf{S}_{22}\end{bmatrix}\begin{Bmatrix}\boldsymbol{\delta}\\ \boldsymbol{\theta}\\ \mathbf{P}\\ \mathbf{M}\end{Bmatrix}, \tag{10}$$

where

$$\mathbf{S}_{11} = \begin{bmatrix} 0 & \tau & -\kappa & 0 & 1 & 0 \\ -\tau & 0 & 0 & -1 & 0 & 0 \\ \kappa & 0 & 0 & 0 & 0 & 0 \\ 0 & 0 & 0 & 0 & \tau & -\kappa \\ 0 & 0 & 0 & -\tau & 0 & 0 \\ 0 & 0 & 0 & \kappa & 0 & 0 \end{bmatrix} = -\mathbf{S}_{22}^{\mathrm{T}} \tag{11}$$

and

$$\mathbf{S}_{12} = \begin{bmatrix} 1/GA\gamma & 0 & 0 & 0 & 0 & 0 \\ 0 & 1/GA\gamma & 0 & 0 & 0 & 0 \\ 0 & 0 & 1/EA & 0 & 0 & 0 \\ 0 & 0 & 0 & 1/EI_u & 0 & 0 \\ 0 & 0 & 0 & 0 & 1/EI_v & 0 \\ 0 & 0 & 0 & 0 & 0 & 1/GI_w \end{bmatrix}. \tag{12}$$

In the D'Alembert view of dynamic equilibrium of equation (10), inertia forces are considered to act in opposition to elastic forces. Introducing the inertia forces into equation (10) yields the governing partial differential equations for the dynamic equilibrium as

$$\frac{\partial}{\partial s}\begin{Bmatrix} \boldsymbol{\delta} \\ \boldsymbol{\theta} \\ \mathbf{P} \\ \mathbf{M} \end{Bmatrix} = \begin{bmatrix} \mathbf{S}_{11} & \mathbf{S}_{12} \\ \mathbf{0} & \mathbf{S}_{22} \end{bmatrix}\begin{Bmatrix} \boldsymbol{\delta} \\ \boldsymbol{\theta} \\ \mathbf{P} \\ \mathbf{M} \end{Bmatrix} + \begin{bmatrix} \mathbf{0} & \mathbf{0} \\ \mathbf{T}_{21} & \mathbf{0} \end{bmatrix}\frac{\partial^2}{\partial t^2}\begin{Bmatrix} \boldsymbol{\delta} \\ \boldsymbol{\theta} \\ \mathbf{P} \\ \mathbf{M} \end{Bmatrix}, \tag{13}$$

where

$$\mathbf{T}_{21} = \begin{bmatrix} \rho A & 0 & 0 & 0 & 0 & 0 \\ 0 & \rho A & 0 & 0 & 0 & 0 \\ 0 & 0 & \rho A & 0 & 0 & 0 \\ 0 & 0 & 0 & \rho I_u & 0 & 0 \\ 0 & 0 & 0 & 0 & \rho I_v & 0 \\ 0 & 0 & 0 & 0 & 0 & \rho I_w \end{bmatrix}. \tag{14}$$

Equation (13) describes the dynamic behaviour of a helical spring and is essentially the same as Wittrick's governing differential equations [3].

2.3. DISPERSION RELATIONSHIP

These equations are now solved to find free wave solutions. A wave in the spring is composed of temporal and spatial variation. The temporal variation is characterized by the angular frequency ω and the spatial variation is characterized by the wavenumber k, where k is taken as real for an exponentially decaying wave and imaginary for a propagating wave.

In a free wave, the translational and rotational motions and the stress for an element of the wire all have the same spatial dependence, so if the responses of an element of the wire

are harmonic in time, we write the displacements and forces for a particular free wave as

$$\begin{Bmatrix} \boldsymbol{\delta} \\ \boldsymbol{\theta} \\ \mathbf{P} \\ \mathbf{M} \end{Bmatrix} = \begin{Bmatrix} \Delta \\ \Theta \\ \Pi \\ \Lambda \end{Bmatrix} e^{ks + j\omega t}. \tag{15}$$

Substituting equation (15) into equation (13) gives a set of 12 homogeneous linear simultaneous equations,

$$\left(k[\mathbf{I}] - \begin{bmatrix} \mathbf{S}_{11} & \mathbf{S}_{12} \\ \mathbf{S}_{21} & \mathbf{S}_{22} \end{bmatrix} \right) \begin{Bmatrix} \Delta \\ \Theta \\ \Pi \\ \Lambda \end{Bmatrix} = \mathbf{0}, \tag{16}$$

where $\mathbf{S}_{21} = -\omega^2 \mathbf{T}_{21}$. In order that equation (16) should have a non-zero solution, it is necessary for the determinant of the matrix $(k[\mathbf{I}] - \mathbf{S})$ to vanish. This is an ordinary eigenvalue problem of dimension 12. It follows that there are 12 wavenumbers, six relating to the forward direction and six to backward direction velocities of wave propagation. If the frequency is given, the free wavenumbers can be found from the eigensolutions of the system matrix of equation (16). The eigenvectors $\{\Delta \Theta \Pi \Lambda\}^{\mathrm{T}}$ represent the deformation and stresses associated with free wave propagation at wavenumber k and frequency ω.

2.4. DYNAMIC STIFFNESS MATRIX

In this section, the above free wave solutions are used to derive the dynamic stiffness matrices [19] for the helical spring. The relations between loads and displacements at position s are obtained from the first six rows of equation (13):

$$\begin{Bmatrix} \mathbf{P} \\ \mathbf{M} \end{Bmatrix} = -[\mathbf{S}_{12}]^{-1}[\mathbf{S}_{11}] \begin{Bmatrix} \boldsymbol{\delta} \\ \boldsymbol{\theta} \end{Bmatrix} + [\mathbf{S}_{12}]^{-1} \frac{\partial}{\partial s} \begin{Bmatrix} \boldsymbol{\delta} \\ \boldsymbol{\theta} \end{Bmatrix}. \tag{17}$$

Next one can write the solution as a sum of 12 waves,

$$\begin{Bmatrix} \boldsymbol{\delta} \\ \boldsymbol{\theta} \end{Bmatrix} = \sum_{i=1}^{12} a_i \{\varphi_i\} e^{k_i s} e^{j\omega t} = [\Phi] \begin{bmatrix} \ddots & & \\ & e^{k_i s} & \\ & & \ddots \end{bmatrix} \{a_i\} e^{j\omega t}, \tag{18}$$

where k_i are the eigenvalues and $[\Phi]$ is the 6×12 eigenvector matrix associated with equation (16) and a_i are the complex amplitudes of the 12 waves. Differentiating equation (18) with respect to s yields

$$\frac{\partial}{\partial s} \begin{Bmatrix} \boldsymbol{\delta} \\ \boldsymbol{\theta} \end{Bmatrix} = [\Phi] \begin{bmatrix} \ddots & & \\ & k_i e^{k_i s} & \\ & & \ddots \end{bmatrix} \{a_i\} e^{j\omega t}. \tag{19}$$

Substituting equation (18) and (19) into equation (17) yields the forces and moments as

$$\begin{Bmatrix} \mathbf{P} \\ \mathbf{M} \end{Bmatrix} = -[\mathbf{S}_{12}]^{-1}[\mathbf{S}_{11}][\Phi]\begin{bmatrix} \ddots & & \\ & \mathrm{e}^{k_i s} & \\ & & \ddots \end{bmatrix}\{a_i\} + [\mathbf{S}_{12}]^{-1}[\Phi]\begin{bmatrix} \ddots & & \\ & k_i \mathrm{e}^{k_i s} & \\ & & \ddots \end{bmatrix}\{a_i\}. \tag{20}$$

Now one can form the 12×1 vector $\mathbf{U}$ of displacements at $s = 0$ and L from equation (18):

$$\mathbf{U} = \begin{Bmatrix} \boldsymbol{\delta}(0) \\ \boldsymbol{\theta}(0) \\ \boldsymbol{\delta}(L) \\ \boldsymbol{\theta}(L) \end{Bmatrix} = \begin{bmatrix} [\Phi] \\ [\Phi]\begin{bmatrix} \ddots & & \\ & \mathrm{e}^{k_i s} & \\ & & \ddots \end{bmatrix} \end{bmatrix}\{a_i\} = \mathbf{D}_1 \mathbf{a}, \tag{21}$$

and the 12×1 vector $\mathbf{F}$ of forces and moments at $s = 0$ and L from equation (20),

$$\mathbf{F} = \begin{Bmatrix} \mathbf{P}(0) \\ \mathbf{M}(0) \\ \mathbf{P}(L) \\ \mathbf{M}(L) \end{Bmatrix} = \begin{bmatrix} -[S_{12}]^{-1}[S_{11}][\Phi] + [S_{12}]^{-1}[\Phi]\begin{bmatrix} \ddots & & \\ & k_i & \\ & & \ddots \end{bmatrix} \\ -[S_{12}]^{-1}[S_{11}][\Phi]\begin{bmatrix} \ddots & & \\ & \mathrm{e}^{k_i L} & \\ & & \ddots \end{bmatrix} + [S_{12}]^{-1}[\Phi]\begin{bmatrix} \ddots & & \\ & k_i \mathrm{e}^{k_i L} & \\ & & \ddots \end{bmatrix} \end{bmatrix}\{a_i\} = \mathbf{D}_2 \mathbf{a}. \tag{22}$$

Here $\mathbf{D}_1$ and $\mathbf{D}_2$ are 12×12 matrices. Eliminating $\mathbf{a}$ from these equations yields the dynamic stiffness matrix $\mathbf{K}$ as

$$\mathbf{F} = \mathbf{K}\mathbf{U} = (\mathbf{D}_2 \mathbf{D}_1^{-1})\mathbf{U}. \tag{23}$$

The matrices $\mathbf{D}_1$ and $\mathbf{D}_2$ contain very large terms associated with wavenumbers with a large positive real part. To avoid numerical problems in inverting $\mathbf{D}_1$, the columns of the eigenvector matrix $[\Phi]$ should be scaled by the factor $\mathrm{e}^{-k_i L}$ for all waves where $\mathrm{Re}(k_i) > 0$. This is possible since eigenvectors have arbitrary scaling.

To use the dynamic stiffness matrix it is necessary to convert from local co-ordinates (u, v, w) to global co-ordinates (x, y, z), apply boundary conditions and solve. One can write a 12×12 matrix

$$\mathbf{T} = \begin{bmatrix} \mathbf{Q}(0) & \mathbf{0} & \mathbf{0} & \mathbf{0} \\ \mathbf{0} & \mathbf{Q}(0) & \mathbf{0} & \mathbf{0} \\ \mathbf{0} & \mathbf{0} & \mathbf{Q}(2n\pi) & \mathbf{0} \\ \mathbf{0} & \mathbf{0} & \mathbf{0} & \mathbf{Q}(2n\pi) \end{bmatrix}^{-1}, \tag{24}$$

where $\mathbf{Q}(\phi)$ is the 3×3 rotation matrix given by equation (3). Then if $\bar{\mathbf{F}}$ is the force vector at the two ends in (x, y, z) co-ordinates and $\bar{\mathbf{U}}$ is the corresponding displacement vector

$$\bar{\mathbf{F}} = \mathbf{TF}, \quad \bar{\mathbf{U}} = \mathbf{TU} \tag{25}$$

and

$$\bar{\mathbf{F}} = \mathbf{TF} = \mathbf{TD}_2\mathbf{D}_1^{-1}\mathbf{U} = \mathbf{TD}_2\mathbf{D}_1^{-1}\mathbf{T}^{-1}\bar{\mathbf{U}}, \tag{26}$$

i.e., in global co-ordinates the dynamic stiffness matrix is

$$\bar{\mathbf{K}} = \mathbf{TD}_2\mathbf{D}_1^{-1}\mathbf{T}^{-1}. \tag{27}$$

2.5. SOLUTION FOR DIFFERENT BOUNDARY CONDITIONS

To find the response of the spring under particular boundary conditions, the matrix $\bar{\mathbf{K}}$ is partitioned and solved by using standard finite element techniques. In order to determine the resonances of the spring, minima are sought in the function

$$\beta = \det|\mathbf{K}'|, \tag{28}$$

where, for free–free boundary conditions, the full matrix $\bar{\mathbf{K}}$ is used. However, for other boundary conditions this has first to be reduced (indicated by $\mathbf{K}'$) by eliminating rows and columns corresponding to clamped degrees of freedom.

It is possible that natural frequencies will be missed by such an approach, particularly if they occur in close pairs. This can be overcome by making use of the Wittrick–Williams algorithm [16], as follows. Denote by $J(\omega)$ the number of natural frequencies of the system below a frequency ω. Consider also the same system but with all the degrees of freedom represented in $\mathbf{K}'$ clamped. The number of natural frequencies of this clamped system below ω is denoted by $J_0(\omega)$. Then if $s\{\mathbf{K}'(\omega)\}$ is the number of negative eigenvalues of the reduced dynamic stiffness matrix $\mathbf{K}'(\omega)$,

$$J(\omega) = J_0(\omega) + s\{\mathbf{K}'(\omega)\}. \tag{29}$$

The method therefore relies on evaluating $s\{\mathbf{K}'(\omega)\}$ as a function of frequency. This can be found by evaluating the eigenvalues of $\mathbf{K}'(\omega)$ or simply by a Gaussian elimination procedure [16]. From equation (29), it can be seen that $s\{\mathbf{K}'(\omega)\}$ increases by one at each natural frequency of the system and reduces by one at each natural frequency of the fully clamped system. If both the clamped and unclamped systems have natural frequencies that are close to one another, this pair could be missed. Therefore, one first requires a knowledge of the latter frequencies.

One way around this is to determine $s\{\mathbf{K}'(\omega)\}$ versus frequency for several different boundary conditions. Each result should yield the same set of natural frequencies of the clamped system, so these results can be combined into a single set. The more such results are obtained, the less likely it is that one of the modes will be missed. An alternative approach was used by Pearson and Wittrick [15], in which one particular set of boundary conditions was used, for which the natural frequencies could easily be determined in their case, and hence the clamped natural frequencies could be derived from equation (29) above.

After an initial broad search, each natural frequency of the unclamped system can be found by refining the search to any required precision. In this way the natural frequencies of the fully clamped system are also obtained without the need to resort to internal node points.

To find the modeshape corresponding to a particular natural frequency ω_n, it may be noted that $\mathbf{K}'(\omega_n)$ has a zero eigenvalue at this frequency. Thus,

$$[\mathbf{K}'(\omega_n)]\,\bar{\mathbf{U}} = 0. \tag{30}$$

The associated eigenvector contains the modeshape at the limited set of degrees of freedom contained in $\mathbf{K}'$. Applying displacements corresponding to this eigenvector allows first the wave amplitudes $\{a_i\}$ to be evaluated from equation (21) and thence also the modeshape at arbitrary positions to be found from equation (18).

2.6. INCLUSION OF STATIC PRELOAD

By using the equations of Pearson [11] it is possible to include the effects of a static axial preload P_0 into the above analysis. It is assumed that, in applying the preload, the spring radius R remains constant but the number of turns n increases slightly. This leads to a modified matrix $\mathbf{S}$ by the inclusion of additional terms, as follows:

$$\mathbf{S}_{22} = \begin{bmatrix} 0 & 0 & 0 & 0 & \dfrac{P_0 \sin\alpha}{EI_v} & \dfrac{-P_0\cos\alpha}{GI_w} \\ 0 & 0 & 0 & \dfrac{-P_0\sin\alpha}{EI_u} & 0 & 0 \\ 0 & 0 & 0 & \dfrac{P_0\cos\alpha}{EI_u} & 0 & 0 \\ 0 & \dfrac{P_0\sin\alpha}{GA\gamma} & \dfrac{-P_0\cos\alpha}{EA} & 0 & \dfrac{P_0R\cos\alpha}{EI_v} & \dfrac{P_0R\sin\alpha}{GI_w} \\ \dfrac{-P_0\sin\alpha}{GA\gamma} & 0 & 0 & \dfrac{-P_0R\cos\alpha}{EI_u} & 0 & 0 \\ \dfrac{P_0\cos\alpha}{GA\gamma} & 0 & 0 & \dfrac{-P_0R\sin\alpha}{EI_u} & 0 & 0 \end{bmatrix} - \mathbf{S}_{11}^{\mathrm{T}}, \tag{31}$$

and

$$\mathbf{S}_{21} = \begin{bmatrix} 0 & 0 & 0 & 0 & 0 & 0 \\ 0 & 0 & 0 & 0 & 0 & 0 \\ 0 & 0 & 0 & 0 & 0 & 0 \\ 0 & 0 & 0 & -P_0\sin\alpha & 0 & 0 \\ 0 & 0 & 0 & 0 & -P_0\sin\alpha & 0 \\ 0 & 0 & 0 & 0 & 0 & P_0\cos\alpha \end{bmatrix} - \omega^2\mathbf{T}_{21}. \tag{32}$$

Here $\mathbf{S}_{11}$ and $\mathbf{T}_{21}$ are as defined in equations (11) and (14) respectively. The helix angle α is also modified by the presence of the static preload.

3. RESULTS AND DISCUSSION

3.1. NATURAL FREQUENCIES AND FORCED RESPONSES

In this section numerical results are given for a spring with a wire radius of 6 mm, a coil radius of 65 mm and a height of 320 mm. The spring has six turns giving a helix angle of 7·44°. This is an approximation to an actual spring which forms a part of the front suspension of a mid-sized passenger car, the actual spring having a greater helix angle for the central four turns and a reduced helix angle near the ends. This variation in helix angle is not included in any of the models considered here.

A finite element model of the spring has been assembled by using NASTRAN, composed of 432 two-noded Euler–Bernoulli beams each covering 5° of arc. Natural frequencies are obtained by the modified Householder method. Pearson's transfer matrix method [11] has also been used, in which the overall transfer matrix of the spring has been divided into 32 equal segments in accordance with reference [11]. The dynamic stiffness method, presented in this paper, has been programmed by using MATLAB [20]. It ran in interpretive mode on a PC with 300 MHz clock speed taking about 2 s for each 100 frequency points. The transfer matrix method took about 2·5 times longer. For the current dynamic stiffness method, the natural frequencies are found by the Wittrick–Williams method [16] as discussed in section 2.5. This allows a further considerable increase in the speed of computation compared to the transfer matrix method.

The natural frequencies for various boundary conditions are given in Tables 1–4. There is generally good agreement among the results of the three numerical analysis methods. The dynamic stiffness method presented in this paper gives identical results to the transfer matrix method of reference [11]. Small discrepancies are found with the finite element results, with a mean of 0·2% and a maximum of 0·9%. Also listed in Tables 1–3 are results predicted for purely extensional/torsional modes, using the method of Banerjee and Williams [8].

Figure 3 shows the modeshapes for the first eight modes of the clamped–clamped spring. Modes 1 and 5 are predominantly extensional and modes 4 and 8 are predominantly

TABLE 1

Natural frequencies in Hz of a spring with clamped–clamped boundary conditions; wire of radius $r = 6\ mm$, $R = 65\ mm$, $\alpha = 7{\cdot}44°$, $n = 6$, $\rho = 7800\ kg/m^3$, $E = 2{\cdot}09 \times 10^{11}\ N/m^2$, $v = 0{\cdot}28$; *all modes below* 100 *Hz are shown*

	Finite element method	Transfer matrix method	Dynamic stiffness method	Pure extension/ torsion	Principal motion
1	41·105	40·99	40·994	42·725	Extensional
2	45·212	45·13	45·135	—	Lateral
3	47·049	46·95	46·951	—	Lateral
4	47·785	47·72	47·726	48·348	Torsional
5	81·325	81·09	81·091	85·449	Extensional
6	89·787	88·97	88·976	—	Lateral
7	91·774	91·59	91·586	—	Lateral
8	93·352	93·18	93·173	96·676	Torsional

TABLE 2

Natural frequencies in Hz of a spring with free–free boundary conditions; wire of radius $r = 6\ mm$, $R = 65\ mm$, $\alpha = 7{\cdot}44^\circ$, $n = 6$, $\rho = 7800\ kg/m^3$, $E = 2{\cdot}09 \times 10^{11}\ N/m^2$, $\nu = 0{\cdot}28$; *all modes below* 100 *Hz are shown*

	Finite element method	Transfer matrix method	Dynamic stiffness method	Pure extension/ torsion	Principal motion
1	42·087	41·96	41·962	42·725	Extensional
2	43·386	43·32	43·309	—	Lateral
3	44·184	44·11	44·106	—	Lateral
4	49·445	49·38	49·384	48·348	Torsional
5	81·415	81·18	81·178	85·449	Extensional
6	86·936	86·72	86·721	—	Lateral
7	88·499	88·30	88·303	—	Lateral
8	95·072	94·93	94·927	96·676	Torsional

TABLE 3

Natural frequencies in Hz of a spring with clamped–free boundary conditions, wire of radius $r = 6\ mm$, $R = 65\ mm$, $\alpha = 7{\cdot}44^\circ$, $n = 6$, $\rho = 7800\ kg/m^3$, $E = 2{\cdot}09 \times 10^{11}\ N/m^2$, $\nu = 0{\cdot}28$; *all modes below* 100 *Hz are shown*

	Finite element method	Transfer matrix method	Dynamic stiffness method	Pure extension/ torsion	Principal motion
1	9·4777	9·472	9·4719	—	Lateral
2	9·5054	9·500	9·4998	—	Lateral
3	21·429	21·36	21·359	21·362	Extensional
4	24·194	24·17	24·170	24·169	Torsional
5	42·182	42·10	42·101	—	Lateral
6	42·942	42·86	42·857	—	Lateral
7	63·310	63·11	63·109	64·087	Extensional
8	71·281	71·20	71·205	72·507	Torsional
9	88·435	88·22	88·227	—	Lateral
10	90·095	89·89	89·893	—	Lateral

TABLE 4

Natural frequencies in Hz of a spring with simply supported boundary conditions; wire of radius $r = 6\ mm$, $R = 65\ mm$, $\alpha = 7{\cdot}44^\circ$, $n = 6$, $\rho = 7800\ kg/m^3$, $E = 2{\cdot}09 \times 10^{11}\ N/m^2$, $\nu = 0{\cdot}28$; *all modes below* 100 *Hz are shown*

	Finite element method	Transfer matrix method	Dynamic stiffness method
1	28·571	28·51	28·516
2	29·209	29·17	29·171
3	31·225	31·16	31·162
4	33·811	33·78	33·784
5	70·300	70·13	70·125
6	74·837	74·72	74·721
7	78·253	78·10	78·099
8	79·774	79·63	79·630

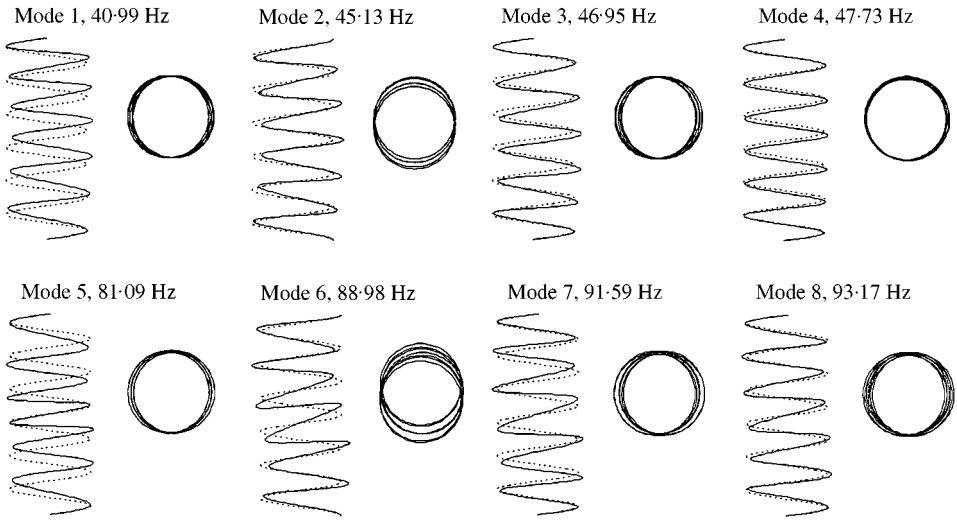

Figure 3. Modeshapes for clamped–clamped boundary conditions, side view and plan view. Solid line: displaced shape, dotted line: undisplaced shape.

torsional. However, the presence of lateral motion can also be observed. The other modes are predominantly lateral in character. Similar results are observed for free–free boundary conditions, but for the clamped–free case, the lateral and axial modes are well separated.

It may be noted from Tables 1 and 2 that both free–free and clamped–clamped boundary conditions result in a cluster of four modes between 40 and 50 Hz and a further four modes between 80 and 95 Hz. Also listed in these tables are results for purely extensional/torsional modes derived using the method of Banerjee and Williams [8]. In the latter case, the free–free and clamped–clamped results are equal (see also reference [9]). In contrast, in the fully coupled results, none of the free–free natural frequencies is equal to any of the clamped–clamped natural frequencies. This shows that coupling between extensional/torsional motion and lateral motion leads to the equality of natural frequencies identified by Williams *et al.* [9] becoming only approximate. This is a consequence of the particular geometry of the spring under study.

Although not equal, the natural frequencies for the free–free and clamped–clamped boundary conditions are found to occur close together (see Tables 1 and 2). This means that, when using the Wittrick–Williams method, for example with an initial frequency resolution of 1 Hz, two natural frequencies would be missed in each case (81 and 88 Hz). This is not surprising since, in the absence of coupling with lateral motion, the extensional/torsional natural frequencies of the free–free and clamped–clamped cases are identical. However, it is possible to overcome this problem by first using the other boundary conditions considered here to identify the clamped–clamped natural frequencies, as described in section 2.5. In particular, the simply supported modes all lie in different frequency bands to the clamped–clamped modes.

3.2. TRANSFER STIFFNESS

At a given frequency of excitation the ratio between force and displacement can be expressed as a complex stiffness. Particularly useful is the transfer stiffness, i.e., the blocked

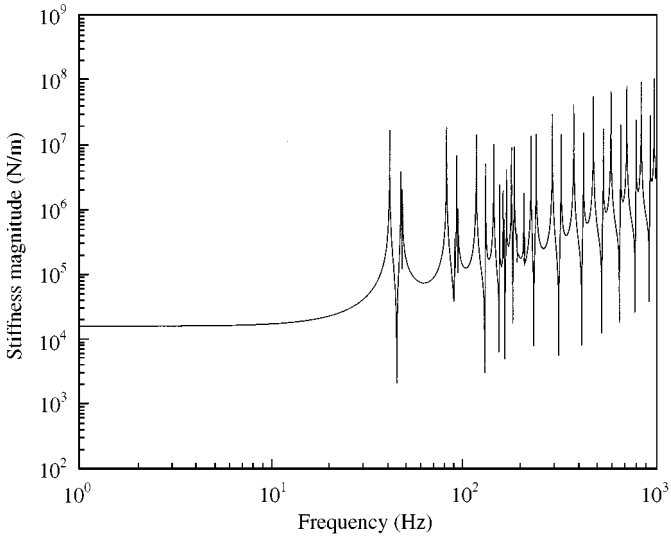

Figure 4. Transfer stiffness of automotive suspension spring in the axial direction predicted by the dynamic stiffness method.

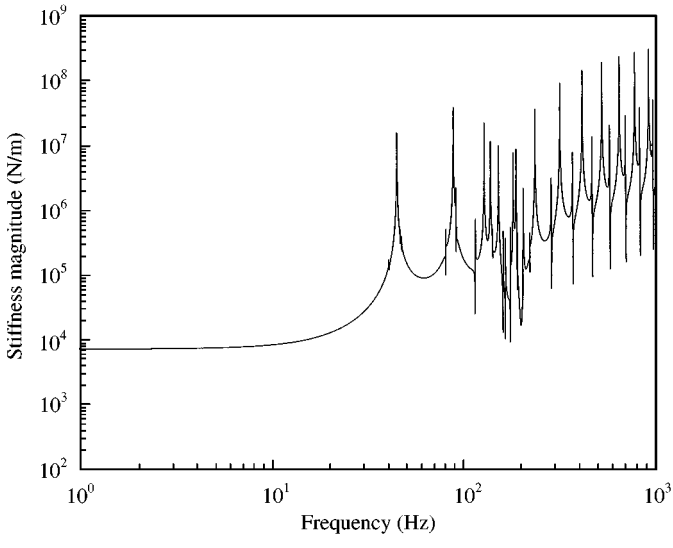

Figure 5. Transfer stiffness of automotive suspension spring in the transverse (y) direction predicted by the dynamic stiffness method.

force at one end due to a displacement input at the other. This can be obtained directly from equation (26) by introducing a displacement vector at one end with only one component non-zero and calculating the force in this direction at the other end. Similarly, by calculating the reaction force at the displaced end, the point stiffness can be obtained.

Figure 4 shows the axial transfer stiffness for the spring under study. A constant damping loss factor of 10^{-3} has been included in these predictions. Results for two directions of transverse stiffness are shown in Figures 5 and 6; the y direction corresponds to a direction

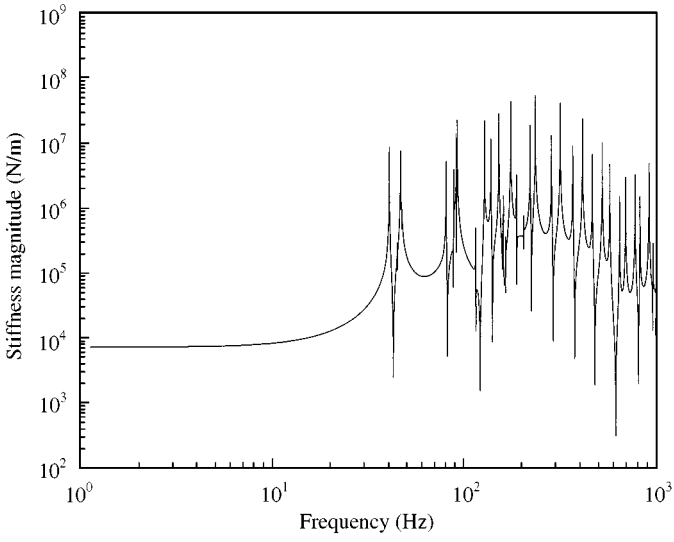

Figure 6. Transfer stiffness of automotive suspension spring in the transverse (z) direction predicted by the dynamic stiffness method.

that is normal to the ends of the wire, whereas the z direction is tangential to the helix (see equation (2)). These two stiffnesses differ considerably at high frequencies. In each direction, the transfer stiffness has a constant quasi-static value at low frequencies, 16·1 kN/m in the axial direction and 7·2 kN/m in the transverse direction. The axial stiffness can be compared with the approximate formula given by Wittrick [3] for small helix angle, $K = GI_w/LR^2$; this gives a value of 15·9 kN/m which agrees closely with the low-frequency limit of the curve in Figure 4.

From about 20 Hz upwards the stiffness increases, with peaks corresponding to various resonances of the clamped–clamped spring. The first two peaks in both the axial stiffness and the transverse stiffness in the z direction are at 41·0 and 46·9 Hz, whereas the first peak in the stiffness in the y direction is at 45·1 Hz. A third peak at 47·7 Hz is also present in the axial stiffness. These are the resonances of the clamped–clamped spring (see Table 1). Compared to the static stiffness, the transfer stiffnesses generally increase at higher frequencies, with a series of peaks and dips caused by resonance behaviour. At the clamped–clamped resonances the stiffness can become very large, limited only by the damping. Unlike a rod, the peaks in the transfer stiffness occur in pairs, with dips between them. This is due to the existence of multiple coupled wave types in the spring.

Due to the coupling between different co-ordinate directions in the coil spring, an axial displacement also produces a transverse force. Other cross-terms in the stiffness matrix are also non-zero. At high frequencies, it is found that these cross-terms can be as large as the direct stiffness terms.

3.3. WAVE PROPAGATION

The dispersion curve, wavenumber versus frequency, gives useful information about the wave propagation. For a given frequency, ω, the harmonic equations of motion were solved to find the complex-valued wavenumber, k from equation (16).

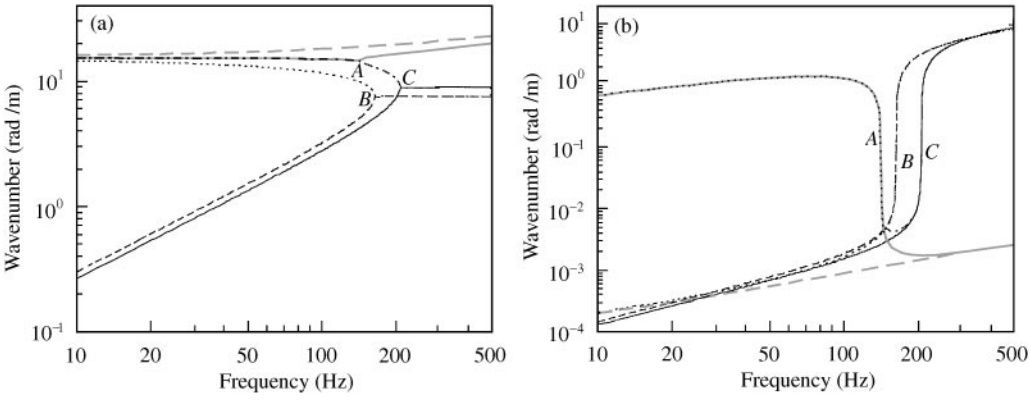

Figure 7. Dispersion curves for spring with helix angle 7·44°. (a) imaginary (propagating) part, (b) real (decaying) part. ——, wave 1; – –, Wave 2; ·····, wave 3; – · –, wave 4; in grey: ——, wave 5; – –, wave 6.

Figure 7 shows the dispersion curves of each motion of the spring. As above, a constant damping loss factor of 10^{-3} has been included in these predictions. Three branch points are labelled A–C. For the spring illustrated, point A occurs at 144 Hz, point B at 166 Hz and point C at 210 Hz. These points separate the frequency range into four regimes. In the first regime, the low-frequency area below point A, travelling waves 1 and 2 start from zero wavenumber at zero frequency. These waves are torsional and extensional waves of the spring respectively. They have similar wavenumbers, as observed by previous authors [4–7], which can induce coupling in modes of a finite spring. Waves 3 and 6 correspond to transverse motion of the wire and start with a wavelength, as measured along the wire, of one revolution of the spring, i.e., a wavenumber of $2\pi n/L$, with n the number of turns. This corresponds to the transverse motion of the whole spring. The near-field waves, 4 and 5, have a large real part, corresponding to decay with distance as well as starting with a wavelength equal to one revolution of the spring. Waves 4 and 5 have the same dispersion characteristics in this region; they are actually complex conjugates of one another.

The dispersion curves can also be used to identify the natural frequencies of various modes approximately. For example, for free–free or clamped–clamped boundary conditions, the first resonances occur when the wavenumber of wave 1 or 2 is approximately equal to π/L or when the wavenumber of wave 3 or 6 differs by approximately $3\pi/2L$ from $2\pi n/L$. The four resulting resonances all occur between 40 and 50 Hz for this particular spring, which leads to the cluster of modes in this frequency region and increases the coupling between extensional/torsional and lateral motion in these modes.

At point A, waves 4 and 5 diverge and change from near-field waves to travelling waves, as indicated by the drop in their real parts. Between points A and B there are therefore six propagating waves. As the wavelength of wave 2 approaches two revolutions of the spring, at point B, its wave type changes from a travelling wave to a near-field wave. Wave 3 also becomes a near-field wave at this point and these two waves form a complex conjugate pair. At point C, the travelling wave 1 also changes to a near-field wave, and wave 4 returns to a near-field wave, these waves again forming a complex conjugate pair. In this high-frequency regime, therefore, there are only two travelling waves, 5 and 6.

The behaviour can also be related to the resonances seen in the stiffness in Figure 4. Between points A and C, 144 and 210 Hz, there is a concentration of resonances, whereas above 210 Hz, where only two propagating wave types remain, the resonances appear more evenly spread.

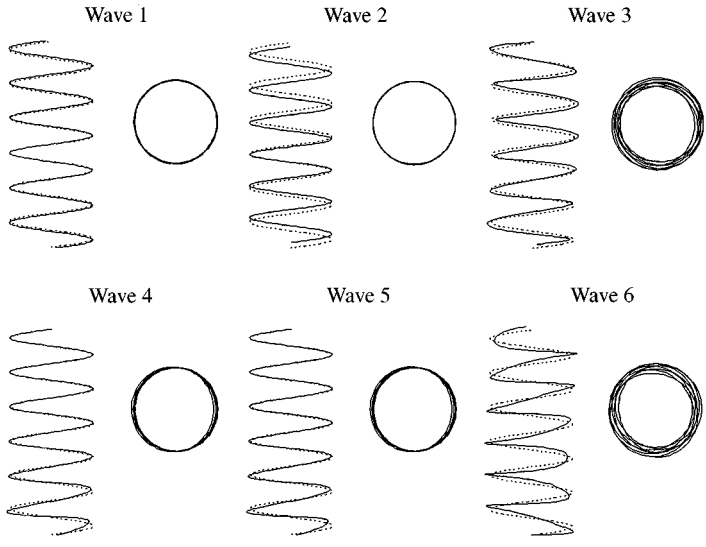

Figure 8. Displacement during free wave motion at 50 Hz. Solid line: displaced shape, dotted line: undisplaced shape.

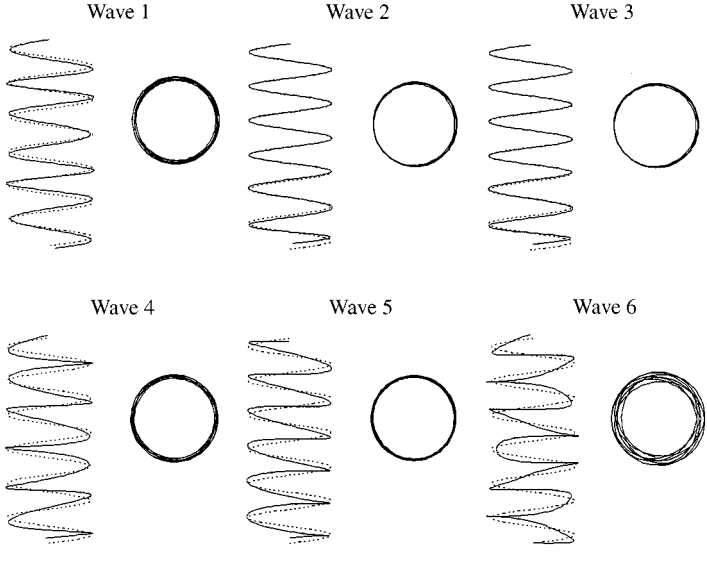

Figure 9. Displacement during free wave motion at 180 Hz. Solid line: displaced shape, dotted line: undisplaced shape.

In order to illustrate the various wave types associated with the dispersion curves, Figures 8–10 show the displacement of the spring at one instant during the various free wave motions. Each figure shows, for each wave, a side view and a plan view of a wave propagating upwards. Six turns are shown, although the free waves apply to an infinite spring. Figure 8 shows results at 50 Hz, representing the low-frequency regime. Waves 1 and 2 can be seen to be torsional and axial waves of the whole spring, with a wavelength of about 8 turns. Waves 3 and 6 are composite wave motions involving lateral motion of the

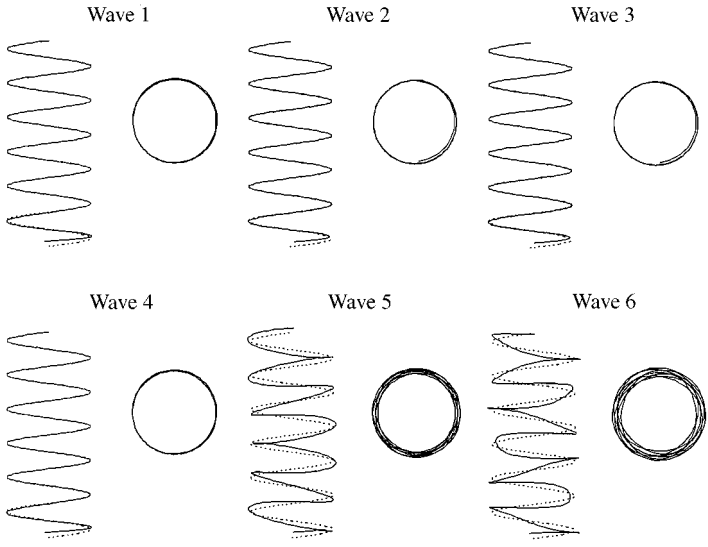

Figure 10. Displacement during free wave motion at 300 Hz. Solid line: displaced shape, dotted line: undisplaced shape.

coils and rotation of the coils about a horizontal axis. Waves 4 and 5 are near-field waves which decay rapidly.

At 180 Hz, Figure 9, the spring is between points *B* and *C*. Waves 4 and 5 have 'cut-on' and are predominantly rotation of the coils about a horizontal axis. Waves 2 and 3 have stopped propagating and are near-field waves. Waves 1 and 6 have a similar nature to the previous figure.

Figure 10 shows the results for 300 Hz, the high-frequency regime. Here, only waves 5 and 6 are propagating waves. Both waves can be excited by both axial and transverse motion.

For the springs studied the effect of shear deformation and rotational inertia is found to be quite small. For propagating waves up to 4 kHz, a difference of at most 1% in the propagating wavenumber and 4% in the decaying (real part) was observed. However, for springs made from a thicker wire the Timoshenko beam formulation is necessary.

3.4. THE EFFECT OF HELICAL ANGLE ON WAVES

As mentioned in the previous section, wave characteristics change at certain transition frequencies. Three non-material parameters, helix angle, helix radius and wire radius, affect these points. The helix angle can have a major effect, whilst the others have less influence [11]. The variations of the dispersion curves of each wave for the spring with helix angle from 0 to 15° are shown in Figure 11. Figure 12 is the plot of the frequency variation of the transition frequencies with helix angle. The number of propagating waves in each region are also marked. For lower values of helix angle an intermediate frequency range exists (between points *A* and *B*) where six propagating wave types can occur, whereas for helix angles above about 8·5° point *A* occurs at a higher frequency than point *B*. As the helix angle increases further, point *A* approaches point *C* and above 15° the distinct transition frequencies at points *A* and *C* cease to exist.

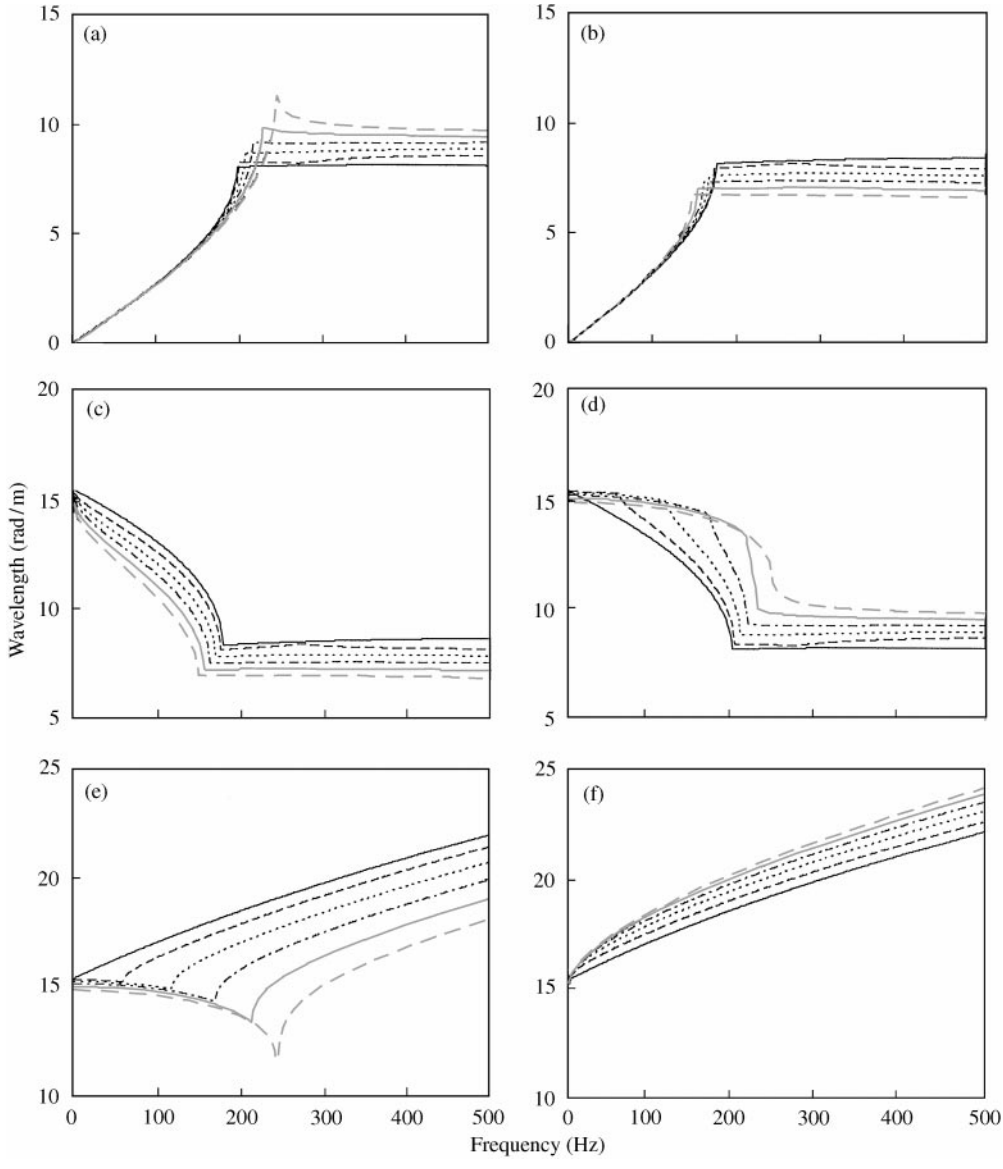

Figure 11. Variation of dispersion curves for each wave with helix angle. —— $\alpha = 0°$; – –, $\alpha = 3°$; ·····, $\alpha = 6°$; – · –, $\alpha = 9°$; in grey; ——, $\alpha = 12°$; – –, $\alpha = 15°$. (a) wave 1, (b) wave 2, (c) wave 3, (d) wave 4, (e) wave 5, (f) wave 6.

Figure 13 shows an example of the dispersion relation for a helix angle of 20°. Waves 2 and 3 cut off at point *B*, leaving two propagating waves at high frequencies, one of which is now wave 1.

3.5. THE EFFECT OF AXIAL PRELOAD

To illustrate the effect of axial preload, the spring has been loaded with 2·5 kN, equivalent to a 49% reduction in its length. The modified transfer stiffness is shown in Figure 14.

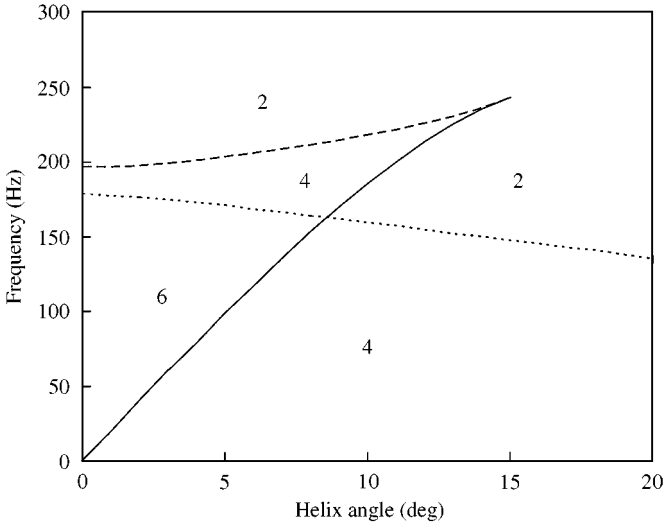

Figure 12. Variation of transition points with helix angle. ——, point A (cut-on of waves 4 and 5), ·····, point B (cut-off of waves 2 and 3), – –, point C (cut-off of waves 1 and 4). Numbers indicate how many propagating waves exist in each region.

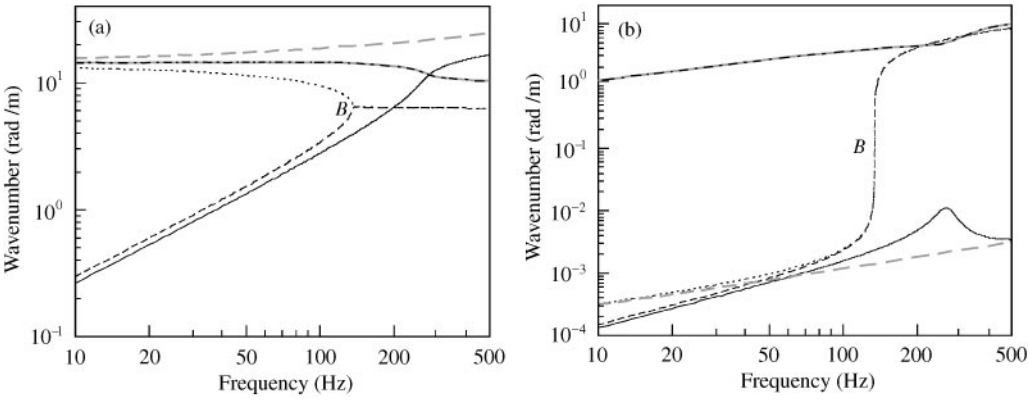

Figure 13. Dispersion curves for spring with helix angle 20°. (a) imaginary (propagating) part, (b) real (decaying) part. ——, wave 1, – – wave 2, ·····, wave 3, – · –, wave 4; in grey: ——, wave 5, – –, wave 6.

This shows that the modal effects occur at slightly lower frequencies, the first three peaks occurring at 36·6, 42·7 and 47·7 Hz. The first two are thus reduced by about 10% whereas the third, the predominantly torsional mode, is unaffected by the preload.

Figure 15 shows the dispersion relation for the compressed spring. Although the spring has a reduced helix angle due to the compression under preload, point A has moved upwards in frequency compared to the result in Figure 7 and is at a higher frequency than point B. Such a trend is comparable to that of *increasing* the helix angle in an unloaded spring (see Figure 12). The increase in the wavenumber of wave 2 at low frequencies corresponds to a reduction in the first extensional natural frequency of the spring. Wave 1 on the other hand, the torsional wave, is unaffected by the preload.

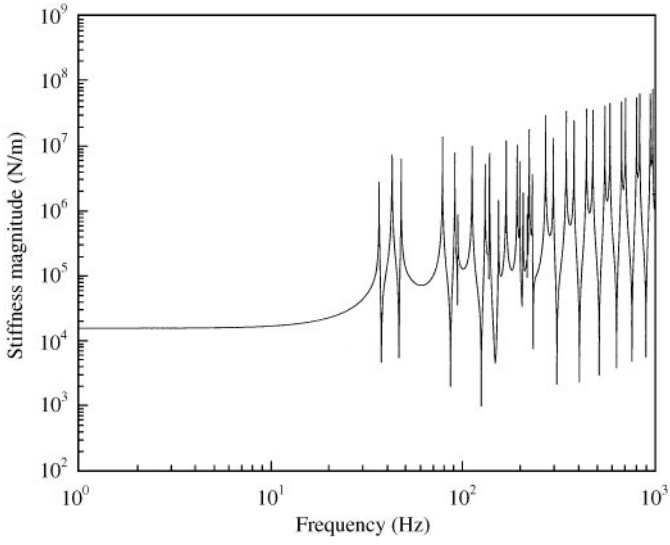

Figure 14. Transfer stiffness of automotive suspension spring in the axial direction for a preload of 2·5 kN.

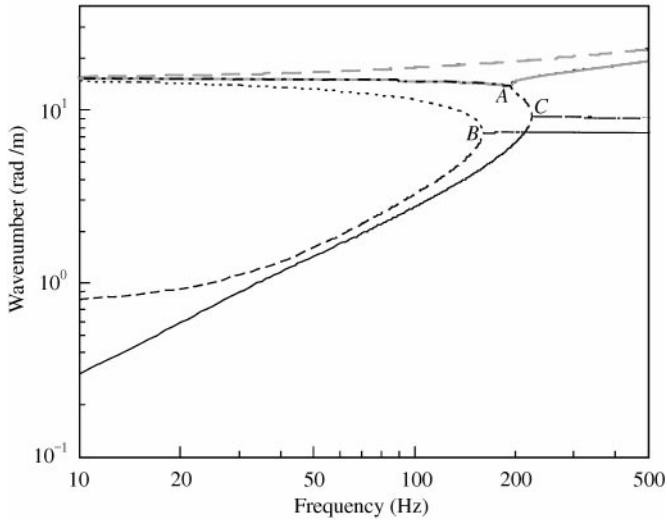

Figure 15. Imaginary (propagating) part of wavenumber for spring with preload of 2·5 kN and loaded helix angle 3·78°. ——, wave 1, – –, wave 2, ·····, wave 3, – · –, wave 4; in grey: ——, wave 5, – –, wave 6.

In Figure 16 the dependence of the three transition frequencies, *A*, *B* and *C* on unloaded helix angle is shown for the situation with preload. In each case, the preload is chosen to give a 49% reduction in length. By comparing this with Figure 12, it can be seen that point *A* is most sensitive to preload, as found in Figure 14, increasing in frequency for a given undeformed helix angle. As a result, the region with six propagating waves only occurs for helix angles less than 6° for this degree of loading, compared to 8·5° for the unloaded case, and points *A* and *B* cease to exist at 11° rather than 15°.

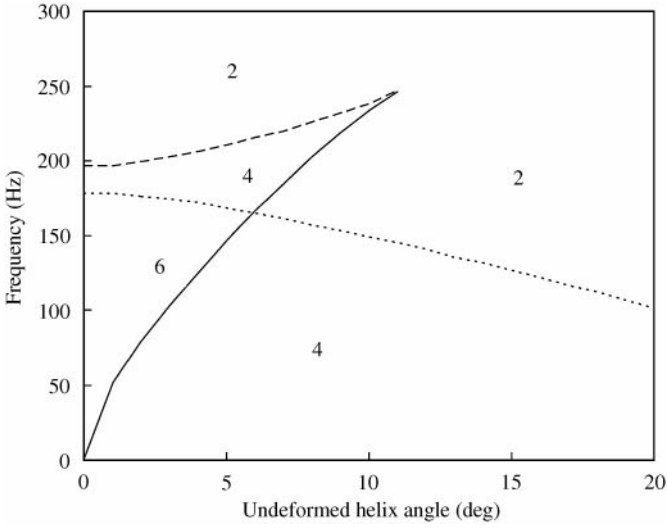

Figure 16. Variation of transition points with undeformed helix angle for a spring loaded to give height reduction of 49%. ——, point A (cut-on of waves 4 and 5), ·····, point B (cut-off of waves 2 and 3), – –, point C (cut-off of waves 1 and 4). Numbers indicate how many propagating waves exist in each region.

4. CONCLUSIONS

The equation of free wave motion in a helical spring, derived from Timoshenko beam theory and Frenet formulae, has been used to obtain the dynamic stiffness matrix. The natural frequencies can be calculated from this matrix, after applying suitable boundary conditions, by using the Wittrick–Williams method. Comparison of the results obtained with those of finite element and transfer matrix calculations show very good agreement. By computing the axial and transverse transfer stiffnesses it has been shown how the spring becomes much stiffer at high frequencies, compared to the static stiffness.

By investigating the dispersion relations in detail it is shown that, while at low frequencies four propagating waves are found, above a certain transition frequency only two remain, which are complex coupled wave types involving both axial and transverse motions. The effect of the helix angle on three different transition frequencies has been investigated. At low helix angles, an intermediate frequency range exists where six propagating wave types can occur; this leads to a clustering of modal peaks in the transfer stiffness. At high helix angles only one of the transition frequencies remains and this clustering does not occur. These effects are also modified by the inclusion of a static preload.

The dynamic stiffness method is an efficient method, particularly suited to the direct calculation of the transfer stiffnesses of a spring in multiple directions. For a typical automotive suspension spring, significant dynamic stiffening has been shown to occur at frequencies as low as 40 Hz, due to internal resonances of the spring. The transfer stiffnesses calculated by using this method, along with the associated direct stiffnesses, could easily be implemented in a fuller, for example multi-body, model of a vehicle. They contain considerably more complex behaviour than would be obtained from a simple rod model of the axial frequency-dependent stiffness.

ACKNOWLEDGMENTS

This work was carried out while the first author was a visiting research fellow at ISVR, Southampton, sponsored by a fellowship from the Korean Science and Engineering Foundation.

REFERENCES

1. A. E. M. LOVE 1899 *Transactions of the Cambridge Philosophical Society* **18**, 364–374. The propagation of waves of elastic displacement along a helical wire.
2. S. P. TIMOSHENKO 1936 *Theory of Elastic Stability*, *New York and London*: *McGraw Hill*. First edition.
3. W. H. WITTRICK 1966 *International Journal of Mechanical Sciences* **8**, 25–47. On elastic wave propagation in helical springs.
4. A. M. WAHL 1963 *Mechanical Springs*, *New York*: *McGraw Hill*. Second edition.
5. W. JIANG, W. JONES, K. WU and T. WANG 1989 *Proceedings of the* 30*th AIAA/ASME/ASCE/AHS/ASC Structures*, *Structural Dynamics and Materials Conference*, *Mobile*, *AL April* 1989, 386–395. Non-linear and linear, static, and dynamic analyses of helical springs.
6. W. JIANG, W. K. JONES, T. L. WANG and K. H. WU 1991 *Transactions of the ASME* **58**, 222–228. Free vibration of helical springs.
7. S. K. SINHA and G. A. COSTELLO 1978 *International Journal for Numerical Methods in Engineering* **12**, 949–961. The numerical solution of the dynamic response of helical springs.
8. J. R. BANERJEE and F. W. WILLIAMS 1994 *Computers and Structures* **50**, 161–166. An exact dynamic stiffness matrix for coupled extensional–torsional vibration of structural members.
9. F. W. WILLIAMS, W. P. HOWSON and J. R. BANERJEE 1993 *Journal of Sound and Vibration* **165**, 373–375. Natural frequencies of members with coupled extension–torsional motion: a physical approach.
10. J. E. MOTTERSHEAD 1980 *International Journal of Mechanical Sciences* **22**, 267–283. Finite elements for dynamical analysis of helical rods.
11. D. PEARSON 1982 *Journal of Mechanical Engineering Science* **24**, 163–171. The transfer matrix method for the vibration of compressed helical springs.
12. VEBIL YILDIRIM 1996 *International Journal for Numerical Methods in Engineering* **39**, 99–114. Investigation of parameters affecting free vibration frequency of helical springs.
13. V. YILDIRIM and N. INCE 1997 *Journal of Sound and Vibration* **204**, 311–329. Natural frequencies of helical springs of arbitrary shape.
14. VEBIL YILDIRIM 1999 *International Journal of Mechanical Sciences* **41**, 919–939. An efficient numerical method for predicting the natural frequencies of cylindrical helical springs.
15. D. PEARSON and W. H. WITTRICK 1986 *International Journal of Mechanical Sciences* **28**, 83–96. An exact solution for the vibration of helical springs using a Bernoulli–Euler model.
16. W. H. WITTRICK and F. W. WILLIAMS 1971 *Quarterly Journal of Mechanics and Applied Mathematics* **24**, 263–284. A general algorithm for computing natural frequencies of elastic structures.
17. E. KREYSZIG 1993 *Advanced Engineering Mathematics*, New York: Wiley. 471, Seventh edition.
18. C. E. S. CESNIK, D. H. HODGES and V. G. SUTYRIN 1996 *AIAA Journal* **34**, 1913–1920. Cross-sectional analysis of composite beams including large initial twist and curvature effects.
19. G. B. WARBURTON 1976 *The Dynamical Behaviour of Structures*, Oxford: Pergamon Press. Second edition.
20. *Matlab User's Guide*, version 4, The Math Works Inc., 1992.